International Journal of Rock Mechanics & Mining Sciences 64 (2013) 139–147

Contents lists available at ScienceDirect

International Journal of Rock Mechanics & Mining Sciences

journal homepage: www.elsevier.com/locate/ijrmms

Shear-enhanced compaction in dilating granular materials

Christian Klimczak [a,*], Richard A. Schultz [b]

[a] Department of Terrestrial Magnetism, Carnegie Institution of Washington, 5241 Broad Branch Road, N.W., Washington, DC 20015-1305, USA
[b] ConocoPhillips, PR2010, 600 North Dairy Ashford, Houston, TX 77079, USA

ARTICLE INFO

Article history:
Received 2 July 2012
Received in revised form
19 July 2013
Accepted 4 August 2013

Keywords:
Volumetric deformation
Shear strain
Deformation bands
Dilation bands
Compactive shear bands

ABSTRACT

Compaction of loose, granular materials commonly results in the loss of porosity and, hence, a volumetric decrease of the material by the localization of deformation bands. Different types of deformation bands tend to form at a range of specific angles to maximum compression (σ_1), as documented in numerous field and laboratory studies. Usually, localization of bands occurs at low angles to σ_1 during deformation involving volumetric increase and at higher angles during compaction of the material. Generally in agreement with field and laboratory orientation measurements, several models have been used to obtain the optimum angle deformation band formation with respect to σ_1. However, some field and laboratory studies report deformation bands with substantial compaction across them that have orientations requiring material dilation to be in accord with those models. This discrepancy is explored by modeling the orientations of structures under progressive deformation for all combinations of simultaneous pure and simple shear. Our results allow for shear-enhanced compaction at the onset of dilational shear band formation, thus accounting for both the band orientation as well as the observed compaction within the bands. These findings indicate that compaction localized within a deformation band is not simply related to a total volumetric decrease of the material, since the transition between localization of compaction and dilation is found not to coincide with the transition of volume decrease to increase of the material, and hence to the material's mechanical response at a given stress state.

1. Introduction

Compactional shear bands [1] in the Entrada Sandstone in Arches National Park and near Goblin Valley, Utah, were found to have formed from micro-mechanisms involving substantial porosity reduction by grain crushing [2–4], indicative of a volumetric reduction within the band [e.g. [5]]. However, the orientations of these bands at low angles to maximum compression was related to a dilational material response instead [6]. Interestingly, angular relationships of compactional shear bands from several other localities, compiled in this study, are comparable to those reported from the Entrada Sandstone, indicating that despite the presence of micro-mechanisms indicative of volume decreases across the bands, the initial material response should also have been dilational.

At the scale of an incipient deformation band and with respect to the local stress tensor, volumetric increase within granular materials have been associated with the localization of dilation bands [5]; isochoric deformation, i.e., deformation with no volume change, has been related to the formation of shear bands, and compaction bands are believed to localize in materials undergoing volumetric decrease [1,5,7]. Simultaneous shear and volumetric changes produce dilational or compactional shear bands [1,7] and so-called shear-enhanced compaction bands [e.g. [8]]. Deformation mechanisms in dilation bands include pore growth by disaggregation of grains through grain rolling, grain boundary sliding, and breakage of grain bonding cement. Compaction bands typically display micro-mechanisms such as cataclasis and dissolution transfer [1] that involve physical and chemical porosity decrease by grain breakage and pressure solution, respectively.

Different types of deformation bands tend to develop at specific ranges of angles with respect to the axis of maximum compression, σ_1 (Fig. 1). Pure compaction bands (CB) are generally thought to form approximately perpendicular [9–11], while dilation bands (DB) are considered to form more or less parallel to maximum compression [e.g. [11,12]]. Depending on the stress state and constitutive relations, shearing mode and mixed mode structures can localize at orientations anywhere between 0° and 90° with respect to maximum compression, where compactional shear bands (CSB) [e.g. [6,13–19]] and sheared dilation bands tend to have smaller angles to σ_1 as compared to shear-enhanced compaction bands (SECB) [e.g. [14,16,20]]. For example, several field examples of deformation band orientations with respect to σ_1 are pictured in Fig. 2. Pure compaction bands at Buckskin Gulch, Utah, first described as crooked compaction bands at this field site [21] are localized at ~80°, while shear enhanced compaction bands are oriented at ~40° with respect to maximum compression (Fig. 2a). Sets of compactional

* Corresponding Author. Tel.: +1 202 478 8842; fax: +1 202 478 8821.
E-mail address: cklimczak@ciw.edu (C. Klimczak).

1365-1609/$ - see front matter © 2013 Elsevier Ltd. All rights reserved.
http://dx.doi.org/10.1016/j.ijrmms.2013.08.012

shear bands in the Orange quarry, France, are oriented at 39° to σ_1 (Fig. 2b). A normal fault (F) oriented at 20° to σ_1 is associated with compactive shear bands of orientations of ~25° relative to σ_1 in the Entrada Sandstone near Goblin Valley (Fig. 2c).

Several empirical and theoretical models are used to predict the optimum angle, α, a fault or deformation band would make relative to σ_1 [22–24]. Theoretical predictions may vary by several degrees among those models [23–26], so that different field or laboratory measurements may be described adequately by different models, depending on rock properties and boundary conditions [23,24].

For a first order estimation and with general applicability to a great variety of materials for which volume change during deformation is not considered, the empirical Mohr–Coulomb failure criterion is widely accepted for inferring the orientations of faults or shear bands. Here, the optimum orientations, α_C, of two conjugate planes of shear failure are oriented at angles of $\alpha_C = \pm(\pi/4 - \phi/2)$ relative to maximum compression [27], where ϕ represents the angle of internal friction.

Tying shear deformation band orientation to principal strain increments, the Roscoe orientation, α_R, gives shear band inclinations to σ_1 as a function of the dilatancy angle, ψ, with $\alpha_R = \pi/4 - \psi/2$ [6,28]. For plane strain conditions, the dilatancy angle, as introduced by Hansen [29], represents the ratio of plastic volume change to plastic shear strain [30]. The Roscoe relationship is found to yield good orientation estimates in coarse-grained rock [31] and is consistent with typical orientations of shear-enhanced compaction bands [13].

In light of well-known mismatches between the Mohr–Coulomb and Roscoe relationships to experimental measurements for porous granular materials, a so-called hardening-softening model was developed [30], where both internal friction and dilatancy angles relate to the initial shear band orientation:

$$\sin(90^\circ - 2\alpha) = \sin\left(\frac{\phi+\psi}{2}\right)\cos\left(\frac{\phi-\psi}{2}\right) \quad (1)$$

This relationship reduces to:

$$\alpha = \frac{\pi}{4} - \frac{(\phi+\psi)}{4} \quad (2)$$

if the internal friction and dilatancy angles have comparable values [24,30]. Differences between the results of Eqs. (1) and (2) do not exceed 7° even if values for ψ and ϕ are at a large difference of 90° [24]. The relationship given in Eq. (2) also coincides with the empirically derived function of [32–33] and due to its simplicity and minor deviation from the Mohr–Coulomb model, it is widely used in field and laboratory studies [13,15,23,24,32–35].

From the Drucker–Prager yield surface, strain localization and shear band orientations can also be obtained by [36,37]:

$$\alpha = \frac{\pi}{4} - \frac{1}{2}\arcsin\left(\frac{2(1+\nu)(\mu+\beta) - 3N(1-2\nu)}{3\sqrt{4-3N^2}}\right) \quad (3)$$

where ν is Poisson's ratio, μ is the stress state dependent internal friction coefficient relating to the internal friction angle as $\mu = 2\sqrt{3}\sin\phi/(3 \pm \sin\phi)$ [e.g., [37,38]], and β, the dilatancy factor, relating to ψ in a similar manner than μ to ϕ [e.g., [23,39]]. The variable N is a term related to the deviatoric stress state within the rock relating intermediate deviatoric stress to the von-Mises equivalent stress [e.g., [37]]. The relation described by Eq. (3) is commonly used in numerical modeling applications [13,26,40–42] and for detailed laboratory experiments [11,15–17,43]. Comparison between the Drucker–Prager and the hardening-softening model derived by Vermeer and de Borst [30] shows that both models yield similar shear band orientations for small positive and negative dilatancy angles with reasonable differences even when ψ and ϕ values differ greatly [24].

In the following, we compile the orientations of several sets of deformation bands from field measurements and values reported in the literature. These orientation values are then used to infer dilatancy angles to further explore the relationship of deformation band orientations to volumetric changes of the material.

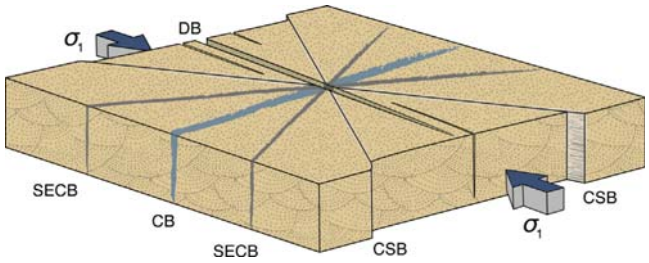

Fig. 1. Schematic of deformation band orientations relative to maximum compression (σ_1).

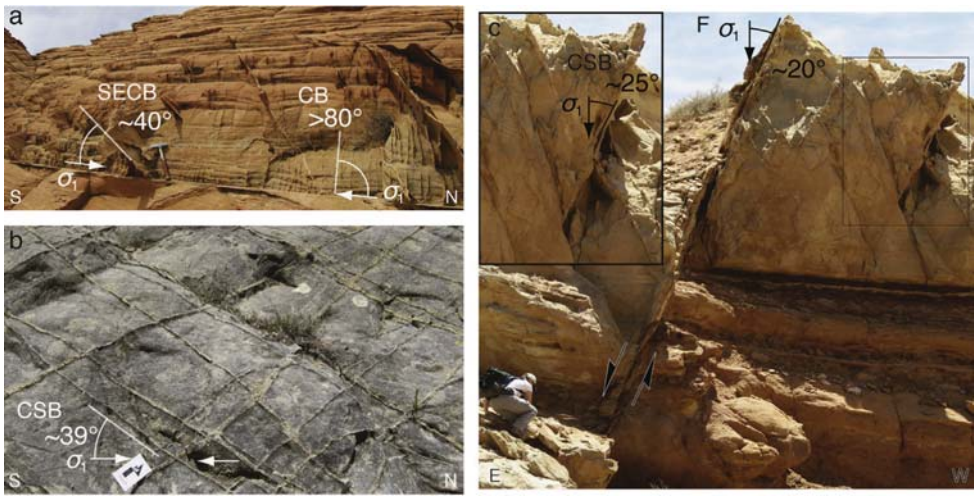

Fig. 2. Fractures and deformation bands relative to maximum compression. (a) Shear-enhanced and pure compaction bands in Navajo Sandstone, Buckskin Gulch, Utah. (b) Compactional shear band network in the Orange quarry, France. (c) Compactive shear bands accompanying a normal fault (F) in the Entrada and Navajo Sandstones, near Goblin Valley, Utah.

2. Orientations of deformation bands and their relation to volumetric deformation

For angles of internal friction of $\phi \sim 30 \pm 10^\circ$, a range of values not atypical for sands and sandstones [e.g. [25], and dilatancy angles around $\psi = 0^\circ$, Eq. (1) predicts shear bands to grow at angles to σ_1 of $\alpha \sim 37.5 \pm 9^\circ$ [13]. Predictions for similar assumptions with the Drucker–Prager derived orientation model (Eq. (3)) using values for Poisson's ratio of $\nu = 0.2$ and an axisymmetric compressional stress state of $N = 1/\sqrt{3}$ yield slightly higher angles to σ_1 of $\alpha \sim 41^\circ$. This suggests that, under such conditions and material properties, deformation bands forming in materials with negative dilatancy angles should form with inclinations to σ_1 that are greater than $\alpha \sim 37.5$–41°, whereas bands forming in materials with positive dilatancy angles should have inclinations smaller than $\alpha \sim 37.5$–41°.

Shear band orientations for the Drucker–Prager derived orientation model not only depend on the dilatancy and friction coefficients but also on the deviatoric stress state, N (Eq. (3)), where $N = 1/\sqrt{3}$ represents axisymmetric compression and $N = -1/\sqrt{3}$ represents axisymmetric extension [e.g. [37]]. The effect of N on band orientation for a given range of dilatancy factors and for several frictional properties are highlighted in 3D space (Fig. 3). For examples considering constant friction coefficients of $\mu = 1$ and $\mu = -1$ (Fig. 3a), a constant friction coefficient obtained for a friction angle of $\phi = 30$ (Fig. 3b), and the case of $\mu = \beta$ (Fig. 3c), the effect of N is negligible for the midrange of dilatancy factors ($-1 < \beta < 1$) and becomes somewhat important for deformation band orientations for dilatancy factors in the higher positive and negative ranges. This shows that shear band inclinations smaller than $\alpha \sim 37.5$–41° for the above inferred conditions are associated with a positive dilatancy more or less independent of N (Fig. 3b).

Following Johnson's approach [6], we measured deformation band orientations of sets of bands with conjugate geometries in the Orange quarry, France [13,44], the Subhercynian Cretaceous Basin, Germany [19], and a sand pit near Freden, Germany [45] (Table 1). These orientations were used to infer the angular relationship of the bands relative to the geologically inferred axis of maximum compression [e.g., [10,13,19], given that the magnitudes of the causative stress states are not well constrained. We then calculated the dilatancy angles from Eq. (1) and list the observed deformation micro-mechanism for comparison.

From the Orange quarry, two generations of bands are reported in [13], of which the bands of the older generation show orientations to σ_1 of 45° and the younger generation show orientations of 39°. These orientations predict negative dilatancy angles for internal friction angles of $\phi = 30^\circ$ (Table 1). Both generations of bands are cataclastic [13,46]. Compactional shear band orientations were measured at 18 localities along a deformation band damage zone in the Subhercynian Cretaceous Basin. Orientations with respect to σ_1 range from 22.6° to 44.6°, suggesting a range of dilatancy angles of -28° to 65°. All bands show deformation micro-mechanisms that point to a localized volume loss, such as cataclasis and pressure solution [19] within the bands, whereas dilatancy angles are negative at only seven localities (Table 1). Deformation band orientations measured at five locations within the Freden sand pit are inclined at 24° to 35° to σ_1, which corresponds to positive dilatancy angles. The reported deformation micro-mechanism of grain boundary sliding [45] can be associated with positive or negative volumetric changes of the host rock [1].

In addition to our measurements (Table 1), dilatancy angles can also be inferred for a variety of deformation band orientations reported in the literature (Table 2). Band orientations from Table 2 are shown as a function of the dilatancy angle (ψ inferred from Eq. (1)) for internal friction angles of $\phi = 30^\circ \pm 10^\circ$ (Fig. 4). The data

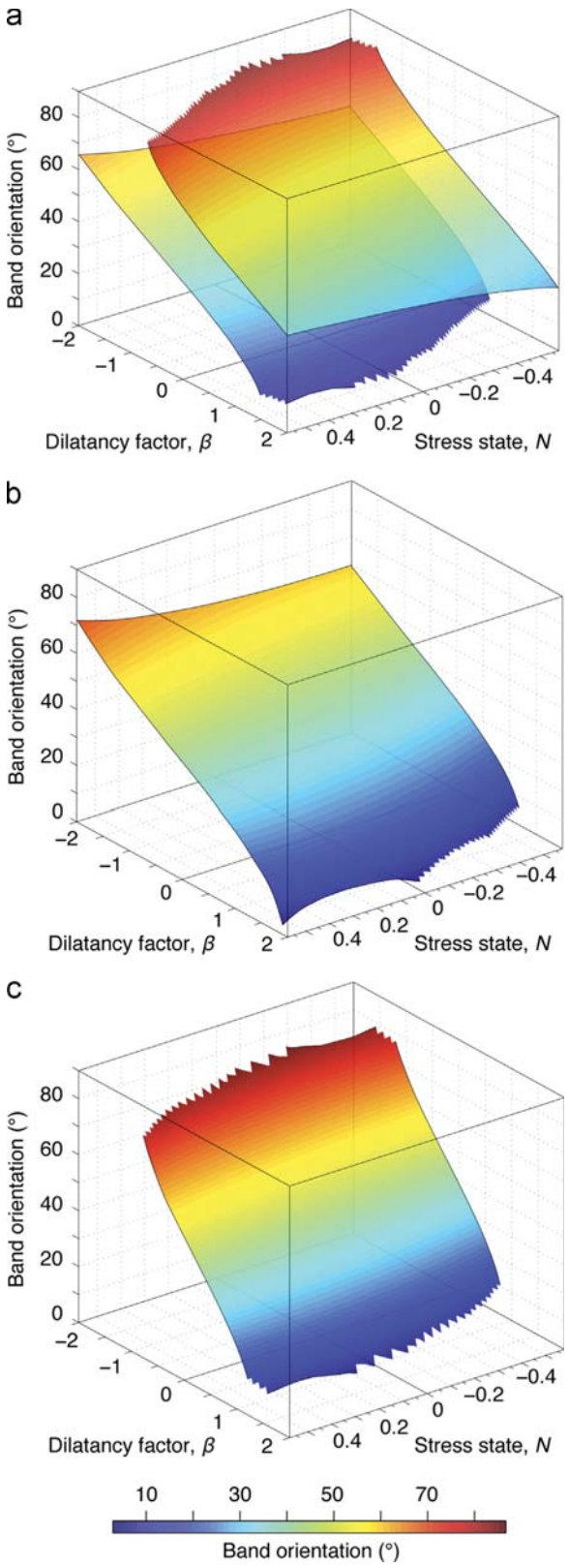

Fig. 3. Shear band orientation (α) of the Drucker–Prager model (Eq. (3)) as function of dilatancy factor and deviatoric stress state. (a) Surfaces of constant friction coefficients of $\mu = -1$ (top) and $\mu = 1$ (bottom). (b) Surface of constant internal friction angle of $\phi = 30^\circ$. (c) Surface of equal friction and dilatancy coefficients representing an associated plastic flow.

points are shown with respect to the Roscoe orientation and to the theoretical orientations predicted by Eqs. (1)–(3). Theoretical predictions are all shown for a constant internal friction angle of

Table 1
Orientations of deformation bands, α, with respect to field estimates of the maximum compression directions.

Location	Measurements	Material	α [°]	ψ[a] [°]	Observed deformation mechanism
Orange quarry, France	1	Sandstone	39 [13]	−5	Cataclasis [13]
	2	Sandstone	45 [13]	−30	Cataclasis [46]
Subhercynian	1	Sandstone	29.3	32.8	Cataclasis, pressure solution [19]
Cretaceous	2	Sandstone	38.6	−3.3	Cataclasis, pressure solution [19]
Basin, Germany	3	Sandstone	38.7	−3.7	Cataclasis, pressure solution [19]
	4	Sandstone	22.6	65.4	Cataclasis, pressure solution [19]
	5	Sandstone	37.9	−0.5	Cataclasis, pressure solution [19]
	6	Sandstone	22.7	64.7	Cataclasis, pressure solution [19]
	7	Sandstone	24.16	56.1	Cataclasis, pressure solution [19]
	8	Sandstone	29.2	33.2	Cataclasis, pressure solution [9]
	9	Sandstone	35.9	7.2	Cataclasis, cementation [19]
	10	Sandstone	42.5	−19	Cataclasis [19]
	11	Sandstone	29.2	33.2	Cataclasis [19]
	12	Sandstone	34.5	12.5	Cataclasis [19]
	13	Sandstone	37	2.9	Cataclasis [19]
	14	Sandstone	26.3	45.6	Cataclasis [19]
	15	Sandstone	44.6	−28.2	Cataclasis [19]
	16	Sandstone	27	42.5	Cataclasis [19]
	17	Sandstone	32.1	21.7	Cataclasis [19]
	18	Sandstone	39.7	−7.6	Cataclasis [19]
Freden pit, Germany	1	Sand	24	57	Grain boundary sliding [45]
	2	Sand	35	10.6	Grain boundary sliding [45]
	3	Sand	29.5	32	Grain boundary sliding [45]
	4	Sand	30.5	28	Grain boundary sliding [45]
	5	Sand	33.5	16.3	Grain boundary sliding [45]

[a] Dilatancy angles obtained from Eq. (1) for internal friction angles of 30°.

Table 2
Compilation of deformation band orientations in sands and sandstones with respect to inferred maximum compression directions.

	Fracture set described as:	Location	Material	α [°]	ψ[b] [°]	Deformation mechanism
O1	Compactional shear bands (Sets N1+S1)	Orange quarry, France	Sandstone	39 [13]	−5	Cataclasis [12]
O2	Compactional shear bands (Sets N2+S2)	Orange quarry, France	Sandstone	45 [13]	−30	Cataclasis [46]
VF1	Shear-enhanced compaction bands (Sets 2+3)	Valley of Fire, NV, USA	Sandstone	38 [14]	−1	Minor cataclasis [14]
VF2	Shear-enhanced compaction bands (Sets 4+5)	Valley of Fire, NV, USA	Sandstone	50 [14]	−58	Minor cataclasis [14]
VF3	Compactional Shear Bands (Set 7+8)	Valley of Fire, NV, USA	Sandstone	32 [14]	22	Strong cataclasis [14]
B	Shear-enhanced compaction bands	Boncavaï quarry, Uchaux, France	Sandstone	43 [10]	−21	Cataclasis [61]
BG	Shear-enhanced compaction bands	Buckskin Gulch, UT, USA	Sandstone	36 [10,20]	6	Cataclasis [21]
GS1[a]	Compactional shear bands	Gosford Sandstone	Sandstone	25 [15]	52	Cataclasis [15]
GS2[a]	Compactional shear bands	Gosford Sandstone	Sandstone	35 [15]	11	Cataclasis [15]
GS3[a]	Compactional shear bands	Gosford Sandstone	Sandstone	26 [15]	47	Cataclasis [14]
SJB	Compactional shear bands	San Juan Basin, NM, USA	Sandstone	30 [18]	30	Cataclasis [18]
][CS1[a]	Compaction bands	Castlegate Sandstone	Sandstone	54 [16]	−68[c]	none reported
CS2[a]	Shear bands	Castlegate Sandstone	Sandstone	25 [16]	77 [c]	none reported
CS3[a]	Compaction bands	Castlegate Sandstone	Sandstone	47 [15]	−27 [c]	none reported
GB	Compactional shear bands	Gruinard Bay, Scotland	Sandstone	26 [47]	47	none reported
SC1	Compactional shear bands	Savage creek, CA, USA	Sand	30 [12,48]	30	Cataclasis [62]
SC2	Dilation bands	Savage creek, CA, USA	Sand	< 20 [12]	77	Dilation [12]
F	Compactional shear bands	Freden pit, Germany	Sand	30.5 [45]	28	Grain boundary sliding [45]
GV	Compactional shear bands	Goblin Valley, UT	Sandstone	25 [6]	52	Cataclasis [2]
SCB	Compactional shear bands	Subhercynian Cretaceous Basin, Germany	Sandstone	33 [19]	19	Cataclasis [19]

[a] From laboratory experiments.
[b] Dilatancy angles obtained from Eq. (1) for internal friction angles of 30°.
[c] Value derived with friction values reported by [16].

$\phi=30°$ to highlight the impact of dilatancy on the orientations of shear bands. The curve for orientations derived from the Drucker-Prager criterion assumes a Poisson's ratio of $\nu=0.2$ and an axisymmetric compressional stress state of $N=1/\sqrt{3}$ [11,22,26,43].

For the same input parameters, the different orientation models yield similar results for dilatancy angles in the range of $-60° < \psi < 60°$ (Fig. 4), a range within which most shear bands considered in this study fall. Major deviations between the models occur at very high or low dilatancy angles ($\psi < -60°$ and $\psi > 60°$). This shows that discriminating between the models becomes problematic when studying the orientations of pure dilation or pure compaction bands.

Orientations of dilation bands [12] are consistent with positive dilatancy angles, whereas compaction band [16] and shear-enhanced compaction band orientations [10,14,20] would be consistent with negative dilatancy angles (Table 2, Fig. 4). Interestingly, many more examples of structures reported as compactional shear bands, which show cataclastic textures within them, have orientations [6,12,14,15,18,47,48] that would require positive dilatancy angles for the range of plausible initial frictional material properties. Some of these bands have such low orientations to σ_1 that they would require positive dilatancy angles greater than 40° (Fig. 4). All considered theoretical and empirical orientation models correlate well with these bands, as all models converge

for the midrange of positive dilatancy angles ($\psi \approx 30^\circ$). This shows that sands and sandstones undergoing deformation with positive dilatancy and friction angles can also develop localized compaction in the form of cataclasis within the bands. This finding highlights that this phenomenon is not unique to the geologic setting and/or rock properties of the Entrada Sandstone in the Goblin Valley area [6] and is consistent with studies of shear and volumetric strains at the onset of shear band localization [11].

In particular, for the compactional shear bands near Goblin Valley, sufficiently low confining pressures were invoked to cause an initial positive dilatancy in the sandstones, and only after the orientation of a band was determined, compaction within the band was inferred to have occurred with grain cracking and the observed cataclasis [6]. In addition, examination of shear band localization based on the Drucker–Prager yield surface [11] showed that porosity reduction in shear bands can be achieved even with small positive dilatancy factors. Such a condition was then interpreted to be met with increasing mean stress with both friction and dilatancy coefficients becoming smaller and/or negative with ongoing deformation.

Evolving dilatancy and frictional properties of sands and sandstones during deformation not only affect each other but also could have an effect on the shear band orientations. In order to explore the shear band orientation as a function of dilatancy angle and to compare the different orientation models, the angle of internal friction was held constant in our analysis. Values used for the angle of internal friction of undeformed sandstones are then interpreted to reflect conditions during the onset of band localization. Changes of the frictional properties with ongoing deformation, such as might be associated with grain fracturing (softening) or interlocking (stiffening) do not modify the shape of the curves derived from Eqs. (1) and (3) (Fig. 3a, Fig. 4) but only result in a shift along the horizontal axis. Maintaining a constant orientation of the deformation band during its growth then requires a corresponding change of the dilatancy angle, where progressively increasing friction angles would require decreasing dilatancy angles with ongoing deformation.

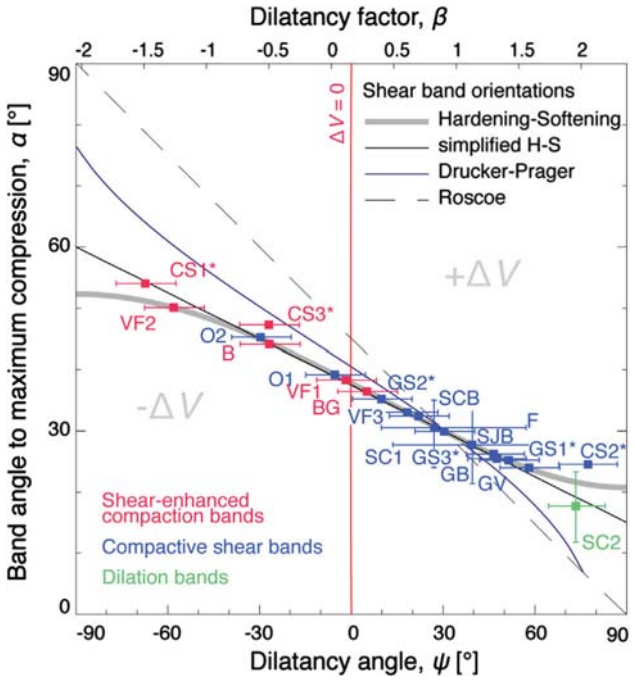

Fig. 4. Band angles to maximum compression shown as a function of the dilatancy and friction angles, where positive dilatancy represents volume increase and negative dilatancy volume decrease of the material.

3. Shear strain within deformation bands during volumetric deformation

Bolton [49] highlighted the mechanical significance of the dilatancy angle by relating the Mohr circle for plane strain increments to simultaneous normal and shear strain and geometrically derived it as the instantaneous angle of motion of two rigid blocks of non-failing granular material relative to a uniformly straining deformation zone that is bound by these two blocks (Fig. 4a). In a similar fashion, Aydin et al. [7] mathematically described deformation bands as a function of the elastoplastic

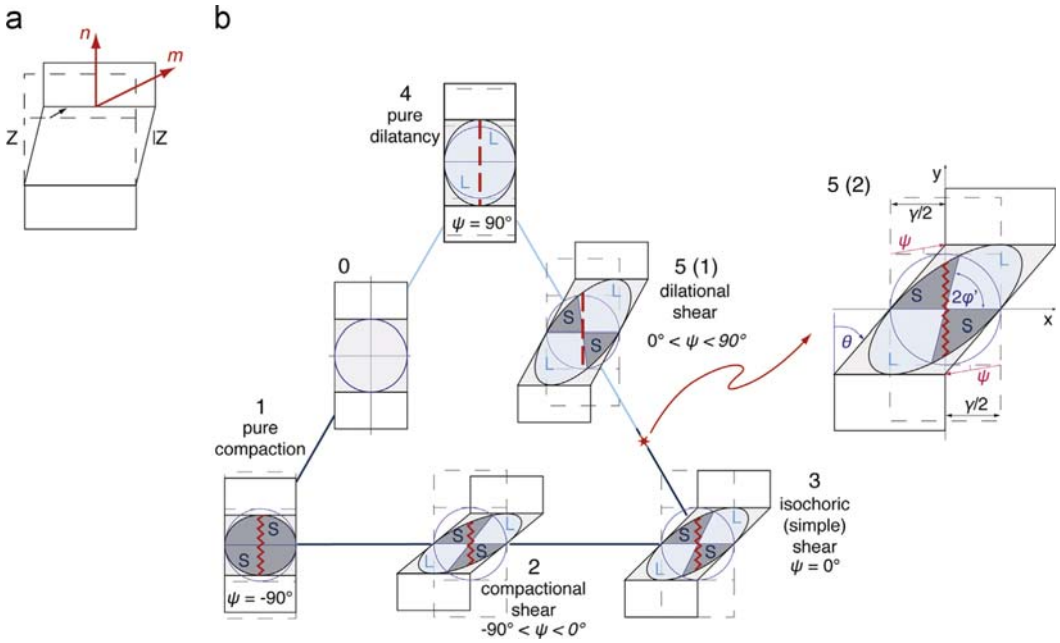

Fig. 5. Block models of simulatanous simple and pure shear. (a) Two rigid blocks bound a uniformly straining deformation zone (ZZ). (b) Strain ellipses of progressive deformation (combined pure and simple shear) adapted to show dilatancy angles and areas of lengthening (L) and shortening (S) across the structure.

acoustic tensor. In their approach, the deformation band type was defined by the angle spanned by the band normal vector (n) and the unit eigenvector of the acoustic tensor (m) that describes the instantaneous direction of the relative velocity jump of the two rigid blocks (Fig. 5a).

The plane strain conditions assumed in our geometric configuration (Fig. 5a) require the deformation zone to coincide with the lines of no extension [49] and thus have orientations to maximum compression following the Roscoe relationship [e.g. [23]]. In addition, the geometrical considerations refer to the instantaneous response of the material at the onset of localization but a detailed consideration of how the material behaves with ongoing deformation (e.g. changing dilatancy and frictional properties) is beyond the scope of this study.

Following both of these models, an increase of the deformation zone width, caused by a positive normal strain component relative to the orientation of the zone, produces a positive local dilatancy angle. Likewise, a decrease of the deformation zone width, caused by a negative normal strain component relative to the deformation zone, produces a negative local dilatancy angle. Applying this geometry to a three dimensional volume of sandstone, where, for the assumed plane strain conditions, no strain is taken to be assumed in the third dimension, the dilatancy angle relates the formation of a deformation zone to volumetric changes within the deformed material. Positive values of the dilatancy angle would then represent a local volumetric increase and negative values would represent a local volume loss within the material [10,50,51]. Aydin et al. [7] relate this to the formation of types of deformation bands and mechanisms, where positive scalar products of $m{\cdot}n$ are found to correspond to dilational shear bands formed by dilational plastic flow, and negative values are found to be associated with compactional shear band formation by compactive plastic flow.

Localized strain during volumetric deformation as described by combinations of local dilatancy and shear angles (Fig. 5b) can be quantified by using the geometry and orientation of the finite strain ellipse (Fig. 5b) of combined pure and simple shear, where the shear angle, θ, is defined as the change in the angle between pairs of lines that are initially perpendicular (Fig. 5b). Strain ellipses highlight areas within the deformation band that are affected by local lengthening, L, and/or local shortening, S, separated by two axes of no normal strain (Fig. 5b). As apparent from the geometric models, the strain expressed along the band-normal vector (n) governs the type of band and its initial style of volumetric change (dilation or compaction), also relating to the size and position of areas of local shortening and lengthening of the strain ellipse for the band.

In accord with the assumed plane strain conditions [49], pure shear is only shown in the y-direction, while simple shear is only shown in the x-direction. Strain ellipses for representative examples throughout the entire range of possible combinations of pure and simple shear, reflecting dilatancy angles from ψ=-90 to +90° (Fig. 5b), indicate that there are five main combinations of local volumetric changes and strain ellipse geometries for deformation bands.

Example 0 in Fig. 5b shows the unstrained geometric setup with a unit circle centered at the location of the deformation zone. *Example 1* shows pure shear only where the bounding blocks of the deformation zone moved toward each other (i.e., a compactional normal strain), resulting in pure compaction, i.e. $\psi=-90°$; $\theta=0°$, and a strain ellipse displaying shortening in all directions other than that parallel to the bounding blocks of the deformation zone. This combination is representative for pure compaction bands and corresponds to $m{\cdot}n=-1$ [7]. *Example 2* depicts compactional shearing as a combination of pure and simple shear with volumetric decrease across the structure, i.e. $\psi<0°$, $\theta>0°$. In this regime, the strain ellipse shows areas of both lengthening and shortening where shortening occurs perpendicular across the deformation zone (Fig. 5b), a setup representative of compactive shear bands that corresponds to $-1<m{\cdot}n<0$ [7]. *Example 3* shows simple shear only, with no volumetric changes, i.e. $\psi=0°$, $\theta>0°$. The strain ellipse is similar to that of *Example 2* (Fig. 5b), where shortening occurs perpendicular across the band. This geometry is consistent with isochoric shearing, where there is no overall volume change—as areas of shortening and lengthening are equal—but compaction enhanced by the simple shear is found perpendicular across the deformation zone. This configuration corresponds to $m\cdot n=0$ [7]. *Example 4* shows pure shear only where deformation zone walls moved away from each other, resulting in pure dilation, i.e. $\psi=90°$, $\theta=0°$. The resulting strain ellipse is lengthened in all directions other than that parallel to the bounding blocks of the deformation zone. The geometric configuration is representative of dilation bands and corresponds to $m\cdot n=1$ [7]. *Example 5* (*1*) points out dilational shearing as a combination of pure and simple shear with volumetric increase across the deformation zone, i.e. $\psi>0°$, $\theta>0°$. The strain ellipse displays areas of shortening and lengthening, with lengthening occurring perpendicular across the zone, representative of dilational shear bands with $0<m{\cdot}n<1$ [7].

Example 5 (*2*) shows that the transition between dilational to compactional shearing need not coincide with the transition between lengthening and shortening across the deformation zone. In fact, geometric configurations applicable to dilational shear bands with $0<m\cdot n<1$ [7] show a shortening perpendicular across the band (Fig. 5b). This implies that dilational shear bands could potentially undergo compaction, enhanced by the shearing, at the onset of their formation. Such initial shear-enhanced compaction might be responsible for observed porosity reduction across some shear bands (Fig. 2a, Fig. 4) also perhaps explaining their low values of orientation to maximum compression.

As shown above, the transition between volumetric changes from dilation to compaction occurs with a dilatancy angle of $\psi=0°$. However, shear-enhanced compaction might occur for positive local dilatancy angles with the transition from shortening to lengthening across a deformation band being marked by an angle between the axes of no length change within the strain ellipse (Fig. 5b) at a value of $2\varphi'=90°$, where φ' represents the orientation of the long axis of the strain ellipse. This transition is primarily dependent on the amount of shear accommodated across the structure and does not coincide with dilatancy angles of $\psi=0°$ (Fig. 5). From Fig. 5b it is apparent that dilatancy and shear angles can be related to the shear strain, γ, as:

$$\gamma=\frac{1}{\frac{1}{\tan\theta}-\tan\psi} \tag{4}$$

Shear strain is related to the orientation of the deformation band strain ellipse as [49]:

$$\varphi'=\arctan\left(\frac{\gamma^2+k_x^2-\lambda_{\max}}{-k_y\gamma}\right) \tag{5}$$

where k_x and k_y represent the stretches in x and y direction, and $\lambda_{\max}$ the eigenvalue of the long axis of the strain ellipse from the two-dimensional deformation matrix [52].

We assumed a unit circle ($r=1$) and no stretch in the y-direction, and computed all possible strain ellipse orientations as a function of the dilatancy angle for the range of possible shear angles (Fig. 6). This computation allows the determination of the range of combinations for which shear-enhanced compaction might occur for positive local dilatancy angles. Within the bounds of geometrically possible angle combinations (Fig. 6, dashed lines), dilational shear, i.e. $0°<\psi<90°$, with shortening across the discontinuity, i.e. $0°\le 2\varphi'<90°$, occurs for a wide range of

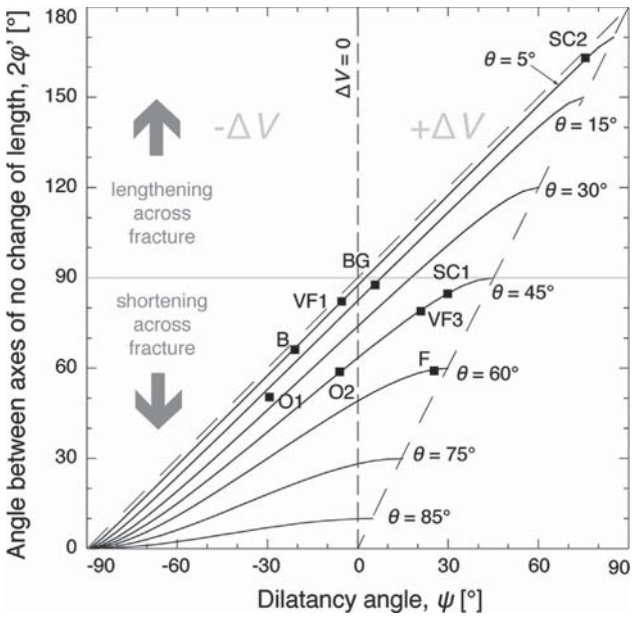

Fig. 6. Total range of orientations of strain ellipses within deformation bands as a function of volumetric changes during deformation (Eq. (4) and (5)). If strain ellipse orientation is $2\varphi' < 90^\circ$, shortening across a band occurs. Note that shortening occurs for a wide range of positive dilatancy angles.

combinations of shear and dilatancy angles. All structures with geometric properties plotting in the fourth quadrant of Fig. 6 show shear-enhanced compaction in a material with positive local dilatancy angles, suggesting this to potentially be a widely occurring phenomenon in nature. Field measurements (Table 1) and literature values (Table 2), for which shear amounts are known, are supportive to the theoretical solution, plotting in the range of dilational shear with shortening across the bands.

Results of this study show that the local shear strain during progressive deformation, involving different combinations of pure and simple shear, has a major impact on the geometry of the resulting localized deformation. It is shown that the range of local dilatancy angles, for which shortening across a deformation band can be accommodated, can include positive values, allowing for shear-enhanced compaction to potentially occur in dilational shear bands. As a consequence, lower values than predictable with the currently established models for orientations of compactive shear bands could be possible. For the range of assumed boundary conditions, shear angles of $\theta \sim 45^\circ$ and positive dilatancy angles, bands can be inclined to σ_1 of as low as $\alpha = 25^\circ$ as predicted by the orientation models (Eqs. (1)–(3)).

4. Discussion and implications

Visualization (Fig. 5) and quantification (Fig. 6) of shear strain at the onset of localized volumetric deformation across deformation bands by relating band geometry to the band-internal strain ellipse show that deformation mechanisms accommodating shortening across a band in the form of shear-enhanced compaction are consistent with a range of local dilatancy angles including positive ones. Hence, observed fracturing mechanisms (e.g., cataclasis) are not necessarily indicative of the initial kinematics of a deformation band or of the initial local volumetric changes within the band. By implication, an in-depth evaluation of simultaneous shear and normal strain conditions in combination with considerations of the influence of pore fluid and stress state effects could increase the understanding of hydraulic properties of sandstones and sands in extensional and compressional tectonic regimes and thus yield further insight into the development of fluid migration pathways in conventional reservoirs.

The onset of compaction localization is usually associated with yielding—the transition between elastic to plastic deformation—of the material, usually represented on an elliptical or tear drop shaped yield envelope [e.g. [53]]. Yield envelopes, commonly plotted in q–p diagrams with the parameters q and p related to shear and mean stresses, are characterized by a positive slope at lower mean stresses and a negative slope, referred to as a cap, at higher mean stresses. Isochoric deformation occurs in the vicinity of the inflection point of the yield curve depending on the details of hardening modulus, stress state, and dilatancy factor. Deformation with local volumetric increases generally occurs where the slope of the yield envelope is positive, while deformation with local volumetric decreases occurs on the yield cap. Localization of compactive shear bands is commonly predicted along the yield cap [7,16,46,53–58]. This requires negative coefficients of friction, which, in turn, predict deformation band orientations with respect to σ_1 at high values, even throughout the range of positive dilatancy factors (Fig. 3a). Observed compactive shear band orientations also include much lower angles, which would require positive friction and positive dilatancy angles (e.g. Table 2). Hence, shear-enhanced compaction, and associated fracturing micromechanisms (i.e., cataclasis), might also occur for conditions found on the positive slopes of the yield envelope, in accord with some previous work.

Further, many constitutive laws to characterize the localization of geologic structures assume associated flow, which is generally defined as having equal friction and dilatancy angles [11] and assuming plastic strain to be approximately normal to the yield surface [27]. In the general case, however, the wide range of possible dilatancy and friction angles (Fig. 4) and the likelihood of a given set of these parameters changing with ongoing deformation indicates that deformation band formation in nature is likely to correspond to non-associated flow. This becomes quite apparent when considering the case where the orientation of deformation bands is locked in at the onset of band formation and stays constant throughout deformation [6]. Strain accumulation within the bands leads to grain fracturing and grain interlocking, hardening and strengthening the initially softer material with ongoing deformation. Such strengthening (increasing friction angle) would then require a decreasing dilatancy angle to maintain a constant band orientation (Fig. 3a, 4).

Under this scenario, cataclastic deformation bands with low angles to maximum compression then might have initially formed under positive local dilatancy and friction, which then could have evolved to negative dilatancy angles with ongoing deformation, causing grain crushing and attendant strain hardening during an advanced stage of the deformation. However, our work shows that for certain combinations of shear and positive dilatancy and friction angles, shear-enhanced compaction is also possible at the onset of the band formation. This then becomes important when considering yield cap models for deformation of soils and porous rock and plays a role in the interpretation of deformation band orientations.

An inference from this study that deformation mechanisms, such as cataclasis, may not be indicative of the initial deformation band kinematics and deformation mechanisms is important when interpreting results obtained from simple band orientation relationships such as those investigated in this paper. The onset of shear-enhanced compaction, for example, depends on the shear distribution during progressive deformation and can also occur during net extension of materials. Similar tendencies are reported for rock fabrics in rift zones, where large-scale regional extension is accompanied by small-scale shortening, evident by both folds and thrust faults [59], as well as for foliations in shear zones undergoing volumetric losses [60].

5. Conclusions

Orientations of different types of deformation bands with respect to maximum compression reveal that a large number of bands, observed to be compactional shear bands that display cataclasis across them, are predicted to form in materials with initial positive dilatancy angles (volume increase) when following several widely accepted relationships of optimum shear band orientations under volumetric deformation. Examination of the range of dilatancy angles for which shortening across the deformation band is possible highlights that observed cataclastic deformation within bands might also be caused by shear-enhanced compaction at the onset of the formation of dilational shear bands. This highlights that deformation micro-mechanisms thought responsible for the localization of compactional shear bands (e.g., cataclasis) can occur for positive dilatancy angles at the onset of deformation, and, hence is not indicative for an overall volumetric decrease of a granular material. This implies that compactive shear bands should also be found on the positive slopes of the yield envelope and that, assuming more or less constant band orientation during deformation, deformation band formation should follow a non-associated flow law. These findings can not only account for the apparent discrepancy of theoretical and observed shear band orientations but also bring detailed insights into fracture geometry development during volumetric deformation.

Acknowledgments

This manuscript has benefitted from comments by an anonymous reviewer and the journal editor. This work was supported in part by NASA's Planetary Geology and Geophysics Program, grant to RAS while the second author was at the University of Nevada, Reno, which is gratefully acknowledged. Additional support was provided by consortium R&D project 429 207806/E20 (IMPACT; http://org.uib.no/cipr/Project/IMPACT) funded by the Research Council of Norway and Statoil. ConocoPhillips is thanked for granting permission to publish this work.

References

[1] Fossen H, Schultz RA, Shipton ZK, Mair K. Deformation bands in sandstone: a review. Journal of the Geological Society 2007;164:755–69.
[2] Aydin A. Small faults formed as deformation bands in sandstone. Pure and Applied Geophysics 1978;116:913–30.
[3] Davis GH. Structural geology of the Colorado Plateau Region of Southern Utah. Geological Society of America Special Paper 1999;342:1–157.
[4] Antonellini MA, Aydin A, Pollard DD. Microstructure of deformation bands in porous sandstones at Arches National Park, Utah. Journal of Structural Geology 1994;16:941–59.
[5] Schultz RA, Fossen H. Terminology for structural discontinuities. American Association of Petroleum Geologists Bulletin 2008;92:853–67.
[6] Johnson AM. Orientations of faults determined by premonitory shear zones. Tectonophysics 1995;247:161–238.
[7] Aydin A, Borja R, Eichhubl P. Geological and mathematical framework for failure modes in granular rock. Journal of Structural Geology 2006;28:83–98.
[8] Wong T-f, Baud P. The brittle–ductile transition in porous rock; a review. Journal of Structural Geology 2012;44:25–53.
[9] Tembe S, Baud P, Wong T-f. Stress conditions for the propagation of discrete compaction bands in porous sandstone. Journal of Geophysical Research 2008;113:B09409.
[10] Fossen H, Schultz RA, Torabi A. Conditions and implications for compaction band formation in the Navajo Sandstone, Utah. Journal of Structural Geology 2011;33:1477–90.
[11] Bésuelle P. Compacting and dilating shear bands in porous rock: theoretical and experimental conditions. Journal of Geophysical Research 2001;106:13435–42.
[12] Du Bernard X, Eichhubl P, Aydin A. Dilation bands: a new form of localized failure in granular media. Geophysical Research Letters 2002;29:2176.
[13] Klimczak C, Soliva R, Schultz RA, Chéry J. Sequential growth of deformation bands in a multilayer sequence. Journal of Geophysical Research 2011;116:B09209.
[14] Eichhubl P, Hooker JN, Laubach SE. Pure and shear-enhanced compaction bands in Aztec Sandstone. Journal of Structural Geology 2010;32:1873–86.
[15] Ord A, Vardoulakis I, Kajewski R. Shear band formation in Gosford sandstone. International Journal of Rock Mechanics and Mining Sciences and Geomechanics Abstracts 1991;28:397–409.
[16] Olsson WA. Theoretical and experimental investigation of compaction bands. Journal of Geophysical Research 1999;104:7219–28.
[17] Olsson WA. Origin of Lüders' bands in deformed rock. Journal of Geophysical Research 2000;105:5931–8.
[18] Olsson WA, Lorenz JC, Cooper SP. A mechanical model for multiply-oriented conjugate deformation bands. Journal of Structural Geology 2004;26:325–38.
[19] Klimczak C, Schultz RA. Fault damage zone origin of the Teufelsmauer, Subhercynian Cretaceous Basin, Germany. International Journal of Earth Sciences (Geologische Rundschau) 2013;102:121–38.
[20] Schultz RA, Soliva R. Propagation energies inferred from deformation bands in sandstone. International Journal of Fracture 2012;176:135–49.
[21] Mollema PN, Antonellini MA. Compaction bands: a structural analog for anti-mode I cracks in aeolian sandstone. Tectonophysics 1996;267:209–28.
[22] Bésuelle P, Rudnicki JW. Localization: shear bands and compaction bands. Geophysical Journal International 2003;89:219–321.
[23] Bardet J. A comprehensive review of strain localization in elastoplastic soils. Computers and Geotechnics 1990;10:163–88.
[24] Bardet J. Orientation of shear bands in frictional soils. Journal of Engineering Mechanics 1991;117:1466–84.
[25] Molenkamp F. Comparison of frictional material models with respect to shear band initiation. Géotechnique 1985;35:127–43.
[26] Schöpfer MP, Childs C. The orientation and dilatancy of shear bands in a bonded particle model for rock. International Journal of Rock Mechanics and Mining Sciences 2012;57:75–88.
[27] Jaeger J, Cook NG, Zimmerman R. Fundamentals of Rock Mechanics. 4th ed. USA/UK/Australia: Wiley-Blackwell; 2007.
[28] Roscoe K. Influence of strains in soil mechanics. Géotechnique 1970;20:129–70.
[29] Hansen B. Line ruptures regarded as narrow rupture zones – basic equations based on kinematic considerations. In: Proceedings of the Brussels Conference on Earth Pressure Problems; 1958.
[30] Vermeer PA, De Borst R. Non-associated plasticity for soils, concrete and rock. Heron 1984;29:1–65.
[31] Vermeer P. The orientation of shear bands in biaxial tests. Géotechnique 1990;40:223–36.
[32] Arthur J, Dunstan T, Al-Ani Q, Assadi A. Plastic deformation and failure in granular media. Géotechnique 1977;27:53–74.
[33] Vardoulakis I. Shear band inclination and shear modulus of sand in biaxial tests. International Journal for Numerical and Analytical Methods in Geomechanics 1980;4:103–19.
[34] Anand L. Onset of shear localization in viscoplastic solids. Journal of the Mechanics and Physics of Solids 1987;35:407–29.
[35] Hobbs B, Mühlhaus H. Instability, softening and localization of deformation. In: Knipe RJ, Rutter EH, editors. Deformation Mechanisms, Rheology and Tectonics. London: The Geological Society; 1990. p. 143–65.
[36] Rudnicki JW, Rice J. Conditions for the localization of deformation in pressure-sensitive dilatant materials. Journal of the Mechanics and Physics of Solids 1975;23:371–94.
[37] Rudnicki J, Olsson W. Reexamination of fault angles predicted by shear localization theory. International Journal of Rock Mechanics and Mining Sciences 1998;35:512–3.
[38] Wong T-f, David C, Zhu W. The transition from brittle faulting to cataclastic flow in porous sandstones: mechanical deformation. Journal of Geophysical Research 1997;102:3009–25.
[39] De Borst R, Groen AE. Some observations on element performance in isochoric and dilatant plastic flow. International Journal for Numerical Methods in Engineering 1995;38:2887–906.
[40] Chemenda AI. The formation of shear-band/fracture networks from a constitutive instability: theory and numerical experiment. Journal of Geophysical Research 2007;112:B11404.
[41] Chemenda AI. The formation of tabular compaction-band arrays: theoretical and numerical analysis. Journal of the Mechanics and Physics of Solids 2009;57:851–68.
[42] Chemenda AI, Wibberley C, Saillet E. Evolution of compactive shear deformation bands: numerical models and geological data. Tectonophysics 2011;526-29:56–66.
[43] Bésuelle P. Evolution of strain localisation with stress in a sandstone: brittle and semi-brittle regimes. Physics and Chemistry of the Earth 2001;26:101–6.
[44] Wibberley CAJ, Petit J-P, Rives T. Mechanics of cataclastic 'deformation band' faulting in high-porosity sandstone, Provence. Earth and Planetary Science 2000;331:419–25.
[45] Brandes C, Tanner DC. Three-dimensional geometry and fabric of shear deformation-bands in unconsolidated Pleistocene sediments. Tectonophysics 2012;518-521:84–92.
[46] Saillet E, Wibberley CAJ. Evolution of cataclastic faulting in high-porosity sandstone, Bassin du Sud-Est, Provence, France. Journal of Structural Geology 2010;32:1590–608.
[47] Healy D, Jones RR, Holdsworth RE. Three-dimensional brittle shear fracturing by tensile crack interaction. Nature 2006;439:64–7.
[48] Imber J, Perry T, Jones RR, Wightman RH. Do cataclastic deformation bands form parallel to lines of no finite elongation (LNFE) or zero extension directions? Journal of Structural Geology 2012;45:158–72.
[49] Bolton M. The strength and dilatancy of sands. Géotechnique 1986;36:65–78.

[50] Cai M, Zhao XG. A confinement and deformation dependent dilation angle model for rocks. American Rock Mechanics Association, 44th US Rock Mechanics Symposium; 2010. 18 pp.
[51] Zhao XG, Cai M. A mobilized dilation angle model for rocks. International Journal of Rock Mechanics and Mining Sciences 2010;47:368–84.
[52] Tikoff B, Fossen H. Simultaneous pure and simple shear: the unifying deformation matrix. Tectonophysics 1993;217:267–83.
[53] Rudnicki JW. Shear and compaction band formation on an elliptic yield cap. Journal of Geophysical Research 2004;109:B03402.
[54] Wong T-f, Baud P. Mechanical compaction of porous sandstone. Oil and Gas Science and Technology 1999;54:715–27.
[55] Karner SL, Chester JS, Chester FM, Kronenberg AK, Hajash Jr. A. Laboratory deformation of granular quartz sand: implications for the burial of clastic rocks. American Association of Petroleum Geologists Bulletin 2005;89:603–25.
[56] Schultz RA, Siddharthan RA. General framework for the occurrence and faulting of deformation bands in porous granular rocks. Tectonophysics 2005;411:1–18.
[57] Grueschow E, Rudnicki J. Elliptic yield cap constitutive modeling for high porosity sandstone. International Journal of Solids and Structures 2005;42:4574–87.
[58] Wibberley CAJ, Petit JP, Rives T. The mechanics of fault distribution and localization in high-porosity sands, Provence, France. Geological Society of London 2007;289:19–46Spec Pub 2007;289:19–46.
[59] Şengör AMC, Bozkurt E. Layer-parallel shortening and related structures in zones undergoing active regional horizontal extension. International Journal of Earth Sciences (Geologische Rundschau) 2013;102:101–19.
[60] Fagereng Å. On stress and strain in a continuous-discontinuous shear zone undergoing simple shear and volume loss. Journal of Structural Geology 2013;50:44–53.
[61] Ballas G, Soliva R, Sizun J-P, Fossen H, Benedicto A, Skurtveit E. Shear-enhanced compaction bands formed at shallow burial conditions; implications for fluid flow (Provence, France). Journal of Structural Geology 2013;47:3–15.
[62] Cashman S, Cashman K. Cataclasis and deformation-band formation in unconsolidated marine terrace sand, Humboldt County, California. Geology 2000;28:111–4.